Supplementary Material for

Octahedral Distortion and Displacement-Type Ferroelectricity with Switchable Photovoltaic Effect in a $3d^3$-Electron Perovskite System

B. W. Zhou,[1,2] J. Zhang,[1,2] X. B. Ye,[1,2] G. X. Liu,[1,2] X. Xu,[1,2] J. Wang,[3] Z. H. Liu,[1,2] L. Zhou,[1] Z. Y. Liao,[1,2] H. B. Yao,[1,2] S. Xu,[1,2] J. J. Shi,[1,2] X. Shen,[1] X. H. Yu,[1,2] Z. W. Hu,[4] H. J. Lin,[5] C. T. Chen,[5] X. G. Qiu,[1,2] C. Dong,[1,2] J. X. Zhang,[3] R. C. Yu,[1,2.6] P. Yu,[7] K. J. Jin,[1,2,6] Q. B. Meng,[1,2] and Y. W. Long[1,2,6,*]

[1]Beijing National Laboratory for Condensed Matter Physics, Institute of Physics, Chinese Academy of Sciences, Beijing 100190, China

[2]School of Physics, University of Chinese Academy of Sciences, Beijing 100049, China

[3]Department of Physics, Beijing Normal University, Beijing 100875, China

[4]Max Planck Institute for Chemical Physics of Solids, Dresden 01187, Germany

[5]National Synchrotron Radiation Research Center, Hsinchu 30076, Taiwan

[6]Songshan Lake Materials Laboratory, Dongguan, Guangdong 523808, China

[7]State Key Laboratory of Low Dimensional Quantum Physics and Department of Physics, Tsinghua University, Beijing, 100084, China

*E-mail: ywlong@iphy.ac.cn

Experimental Methods

Polycrystalline $Hg_{0.75}Pb_{0.25}MnO_3$ (HPMO) was synthesized via a solid-state reaction under high-pressure and high-temperature conditions. Stoichiometric amounts of highly pure (> 99.9%) starting reactants, i.e., HgO, PbO, and MnO_2 at a 3:1:4 molar ratio, were carefully mixed and ground using an agate mortar. The mixed powder was sealed in an Au capsule with a diameter and height of 2.0 mm. All operations mentioned above were performed in a glovebox filled with argon gas. The capsule was treated with a rhenium heater, $LaCrO_3$ thermal isolation sleeve, and MgO octahedron pressure medium on a Walker-type double-stage high-pressure apparatus. Each face of the MgO octahedron pressure medium was pressed by a WC cubic anvil with 4.0 mm corner cuts. Eight cubic anvils were pressed by six first-stage anvils. Once the pressure slowly increased to 15 GPa in 5.5 h, the capsule was heated at 1373 K for 0.5 h. Then, the sample was quenched to room temperature (RT) and the pressure was slowly released to ambient pressure in 14.0 h.

Powder X-ray diffraction (XRD) at RT was performed using a Huber diffractometer with Cu Kα_1 radiation in the 2θ range of 10° to 100° with a step of 0.005°. The crystal structure was resolved by the EXPO2014 program from the XRD data. Rietveld refinement of the XRD data was performed using the FulllProf program [1]. The background was refined by polynomials. The peak profile was refined by the Psudo-Voigt function. X–ray absorption spectra at the Mn-$L_{2,3}$ edges were collected at the BL11A beamline of the NSRRC using the total electron yield mode at RT.

The specimens for transmission electron microscopy (TEM) and scanning

transmission electron microscopy (STEM) were milled and dispersed into high-purity ethanol and transferred on a carbon film with a copper supporting grid. The aberration-corrected TEM and STEM experiments were performed on a JEOL ARM200F transmission electron microscope equipped with double Cs correctors (CEOS) for the condenser lens and objective lens and a cold field-emission gun. High-angle annular dark-field (HAADF) and annular bright-field (ABF) images were acquired at acceptance angles of 11.5-23.0 and 90-370 mrad, respectively. The available spatial resolution for each of the STEM images is better than 78 pm at 200 kV.

Piezoresponse force microscopy (PFM) [2] and atomic force microscopy (AFM) were performed using a commercial scanning probe microscope system (nanoscope-V multimode AFM) equipped with external lock-in amplifiers (SRS 830, Stanford Research Instruments) at RT. Commercially available Si probes coated with Pt (tip radius of < 30 nm, force constant of 5.4 $N \cdot m^{-1}$, and a resonant frequency of 150 kHz) were used to achieve the polarization characterization and switching. The ferroelectric domain structures were imaged at an AC voltage of 1.5 V on the tip. A -5 V bias exceeding the coercive voltage was applied to the tip to switch the downward polarization upward by scanning the surface. All PFM phase images from this study are out-of-plane phase images.

The second harmonic generation (SHG) [3,4] measurement at RT was conducted in a typical reflection geometry, where both the incidence and reflection angle were set at 45°. The incident laser was generated using a Ti: sapphire oscillator (Maitai, Spectra Physics) with a central wavelength of 800 nm (~ 120 fs, 82 MHz). The diameter of the

incident beam was focused to 20 μm before shining onto the sample surface. The setup for applying electric fields was constructed using an Ag/HPMO/Pt structure with the sample of 0.25 mm thick. The laser was set on the side coated with Pt whose thickness was 5 nm for light passing through.

The extinction coefficient κ was obtained by a Kramers–Kronig transformation of the frequency-dependent reflectivity $R(\omega)$ in the range of 400 – 50000 cm^{-1}. Reflectivity data were measured at a near-normal angle of incidence on a Bruker 80v Fourier transform infrared spectrometer using an in situ gold evaporation technique [5]. The reflectivity within the visible-UV range (10000 – 50000 cm^{-1}) was measured with an Avaspec 2048 × 14 optical fiber spectrometer. For the Kramers-Kronig transformation, constant extrapolation was used for $R(\omega)$ below 400 cm^{-1}. Ultimately, the absorption coefficient was obtained according to the equation $\alpha = 4\pi\kappa/\lambda$. Steady-state photoluminescence measurements were performed on an Edinburgh fluorescence spectrometer (FLS 920) by the excitation laser pulses of the pump fluence of ~ 0.5 $nJ \cdot cm^{-2}$ at 445 nm.

The current-voltage and switchable photovoltaic characteristics at RT were collected on a Keithley 2601 B source meter under AM 1.5 G illumination (100 $mW \cdot cm^{-2}$) from a Zolix SS150A solar simulator. The setup for the measurements was constructed using an Ag/HPMO/Ag structure. The electrode spacing of the polycrystalline bulk HPMO sample was 1.2 mm. The area of the Au electrode was 1 mm^2. The light intensity of the solar simulator was calibrated using a standard monocrystalline silicon reference solar cell. The counting interval of current was 0.03125 s. The average rising time of the “on”

curve was about 0.95 s. The average decay time of the “off” curve was about 0.81 s.

Supplementary Table S1. Refined crystallographic parameters of HPMO at room temperature [a)].

parameter	value	parameter	value
Hg/Pb$_y$	0.4708 (1)	Hg/Pb-O1 (Å) × 2	2.39(1)
Hg/Pb$_z$	0.0145(10)	Hg/Pb-O1 (Å) × 2	2.52(1)
Mn$_z$	0.014(3)	Hg/Pb-O1 (Å) × 2	2.81(1)
O1$_x$	0.046(1)	Hg/Pb-O2 (Å)	2.14(1)
O1$_y$	0.204(1)	Hg/Pb-O2 (Å)	2.41(1)
O1$_z$	0.270(2)	Hg/Pb-O2 (Å)	3.02(1)
O2$_y$	0.528(2)	Mn-O1 (Å) × 2	1.77(1)
O2$_z$	0.417(2)	Mn-O1 (Å) × 2	2.06(1)
B for Hg/Pb (Å^2)	1.68(2)	Mn-O2 (Å) × 2	2.02(1)
B for Mn (Å^2)	0.35(4)	Mn-O1-Mn (°)	155.1(5)
B for O1 (Å^2)	3.63(18)	Mn-O2-Mn (°)	149.1(9)
B for O2 (Å^2)	3.63(18)	BVS (Mn)	3.75

[a)]Space group *Ama*2 (no.40); atomic sites are Hg/Pb 4b (0.25, *y*, *z*), Mn 4a (0, 0, *z*), O1 8c (*x*, *y*, *z*), and O2 4b (0.25, *y*, *z*); a = 7.8029(2) Å, b = 5.3312(1) Å, c = 5.2709(2) Å, V = 219.32(1) Å^3, and R_p = 2.21%, R_{wp} = 2.93%. The calculated density is ρ = 9.245 g/cm^3. *B* is the isotropic temperature factor parameter. The occupation factor, *G*, for all atoms was fixed at unity. The BVS values (V_i) were calculated using the formula $V_i = \sum_j S_{ij}$, $S_{ij} = \exp[(r_0 - r_{ij})/0.37]$, and r_0 (Mn^{4+}) = 1.753 Å [6].

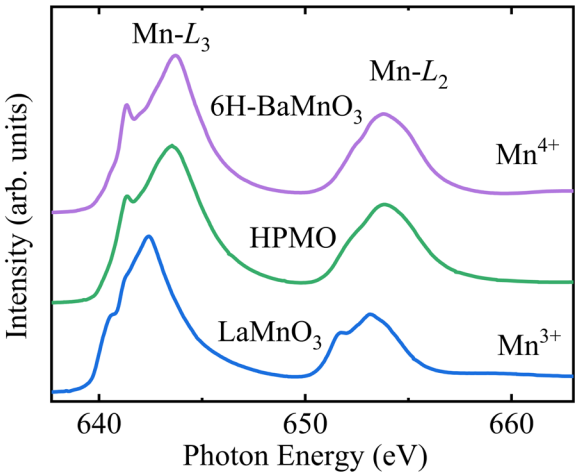

Suppmentary Fig. S1. X-ray absorption spectra at the Mn-$L_{2,3}$ edges for HPMO together with Mn^{3+} reference $LaMnO_3$ [7] and Mn^{4+} reference 6H-$BaMnO_3$ [8] for comparison. The XAS peak profiles and energy positions of HPMO shift toward higher energies by approximately 1.0 eV compared with those of $LaMn^{3+}O_3$ but show very similar characteristic features to those of Mn^{4+} reference 6H-$BaMnO_3$. This result reveals the formation of an Mn^{4+} charge state for HPMO, consistent with the BVS calculations.

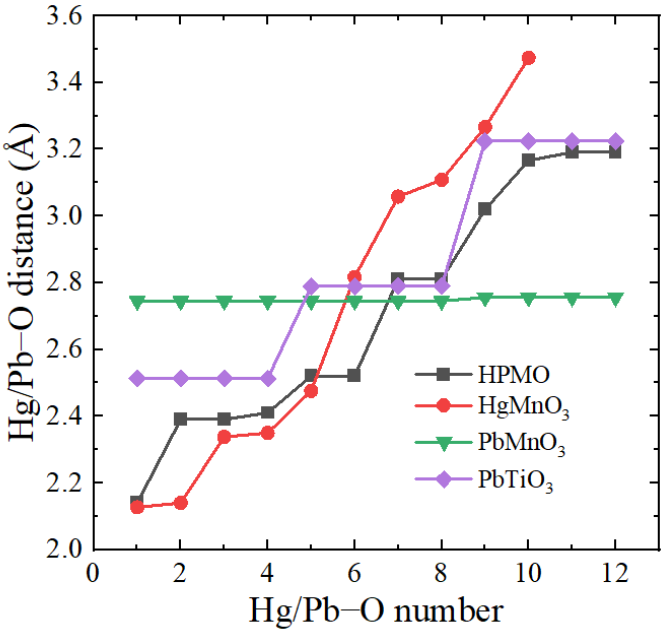

Supplementary Fig. S2. Comparison of the A-site Hg/Pb-O bond lengths for the current HPMO as well as $HgMnO_3$ [9], $PbMnO_3$ [10], and $PbTiO_3$ [11].

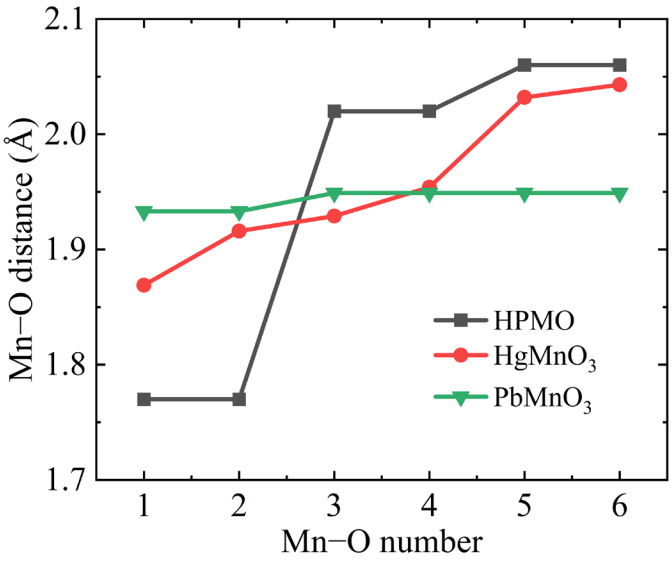

Supplementary Fig. S3. Comparison of the six Mn-O bond lengths for the current HPMO and the two parent phases of $HgMnO_3$ [9] and $PbMnO_3$ [10].

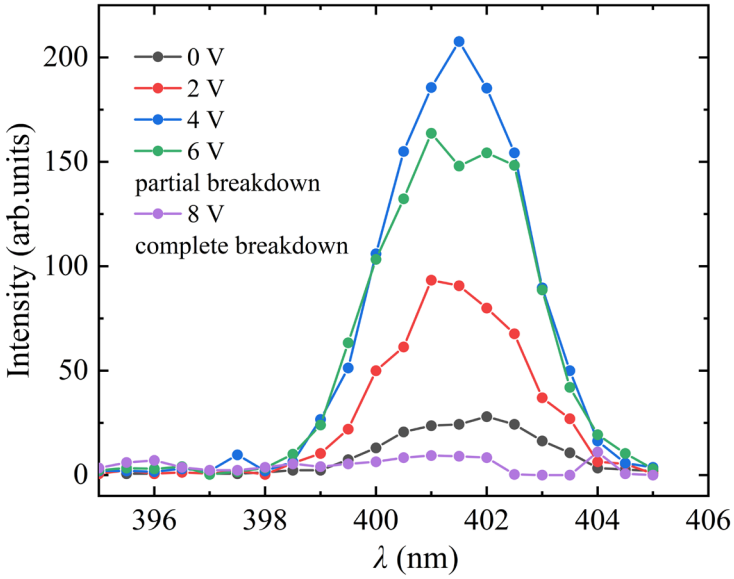

Supplementary Fig. S4. SHG signal measured at different voltages. The sample is partial breakdown as the voltage increases to 6 V, and complete breakdown at 8 V.

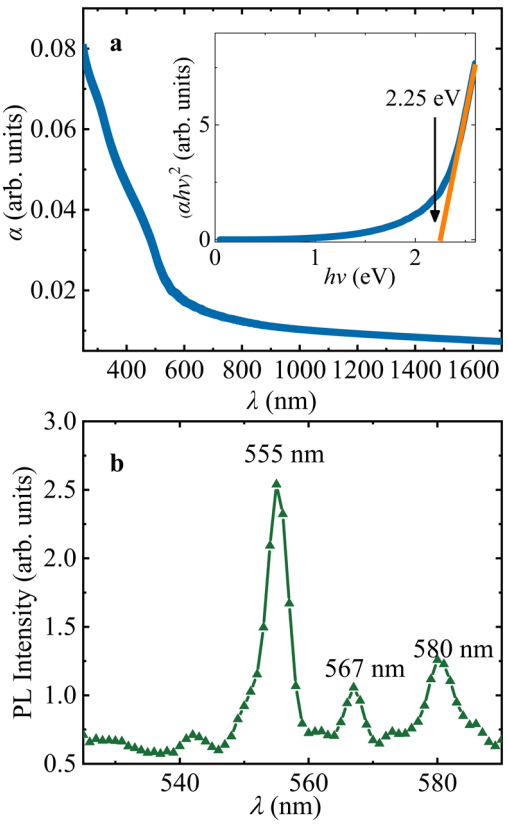

Supplementary Fig. S5. (a) Optical absorption coefficient α for HPMO obtained from reflectivity spectra. The inset shows the direct bandgap plots $(\alpha hv)^2$ versus hv. The spectrum reveals a clear absorption edge in the visible light region. Based on the Tauc and Davis–Mott models [12] shown in the inset, we used the equation $\alpha hv = A(hv - E_g)^{1/2}$ to evaluate the direct bandgap $E_g = 2.25$ eV, which falls into the visible light region. (b) Steady-state photoluminescence (PL) spectrum measured around the bandgap edge. The PL measurements were conducted using a laser source with a wavelength of 445 nm. A strong emission peak near 555 nm that corresponds to the band edge absorption energy of 2.25 eV (~ 552 nm) was found to emerge, manifesting a narrow-line character of free excitons at the absorption edge. Other minor peaks were also observed, probably arising from impurities or defect states around the absorption edge on the polycrystalline sample surface [13].

Reference

[1] J. Rodríguez-Carvajal, Physica B: Condensed Matter. **192**, 55 (1993).

[2] J. X. Zhang *et al.*, Phys. Rev. Lett. **107**, 147602 (2011).

[3] R. Zhao, K. Jin, H. Guo, H. Lu, and G. Yang, Sci. China Phys. Mech. **56**, 2370 (2013).

[4] J. S. Wang *et al.*, Sci. Rep. **7**, 9051 (2017).

[5] C. C. Homes, M. Reedyk, D. A. Cradles, and T. Timusk, Appl. Opt. **32**, 2976 (1993).

[6] I. D. Brown and D. Altermatt, Acta Crystallogr. Sect. B **41**, 244 (1985).

[7] T. Burnus *et al.*, Phys. Rev. B **77**, 125124 (2008).

[8] S. Qin *et al.*, Inorg. Chem. **60**, 16308 (2021).

[9] B. Zhou *et al.*, Inorg. Chem. **59**, 3887 (2020).

[10] X. Li *et al.*, Chem. Mater. **33**, 92 (2021).

[11] K. Shahzad, M. Nasir Khan, G. Shabbir, and J. Bashir, Ferroelectrics. **414**, 155 (2011).

[12] A. Ibrahim and S. K. J. Al-Ani, Czechoslovak J. Phys. **44**, 785 (1994).

[13] S. Seth, T. Ahmed, A. De, and A. Samanta, ACS Energy Lett. **4**, 1610 (2019).